Shear flow-induced motility of *Dictyostelium discoideum* cells on solid substrate

Emmanuel Décavé[1,2], Didier Rieu[1,2], Jérémie Dalous[1], Sébastien Fache[1], Yves Bréchet[3], Bertrand Fourcade[2], Michel Satre[1] and Franz Bruckert[1,*]

[1]Laboratoire de Biochimie et Biophysique des Systèmes Intégrés, Département Réponse et Dynamique Cellulaires, CEA-Grenoble, DRDC/BBSI, 17 rue des Martyrs, 38054 Grenoble Cedex 09, France
[2]Structures et Propriétés des Architectures Moléculaires, Département de Recherche Fondamentale sur la Matière Condensée, CEA-Grenoble, DRFMC/SI3M, 17 rue des Martyrs, 38054 Grenoble Cedex 09, France
[3]Laboratoire de Thermodynamique et de Physico-Chimie du Métal, ENS d'Electrochimie Electrométallurgie, LTPCM, Domaine Universitaire, 38402 Saint-Martin d'Hères, France
*Author for correspondence (e-mail: fbruckert@cea.fr)

Accepted 26 June 2003
Journal of Cell Science 116, 4331-4343 © 2003 The Company of Biologists Ltd
doi:10.1242/jcs.00726

Summary

Application of a mild hydrodynamic shear stress to *Dicytostelium discoideum* cells, unable to detach cells passively from the substrate, triggers a cellular response consisting of steady membrane peeling at the rear edge of the cell and periodic cell contact extensions at its front edge. Both processes require an active actin cytoskeleton. The cell movement induced by the hydrodynamic forces is very similar to amoeboid cell motion during chemotaxis, as for its kinematic parameters and for the involvement of phosphatidylinositol(3,4,5)-trisphosphate internal gradient to maintain cell polarity. Inhibition of phosphoinositide 3-kinases by LY294002 randomizes the orientation of cell movement with respect to the flow without modifying cell speed. Two independent signaling pathways are, therefore, induced in *D. discoideum* in response to external forces. The first increases the frequency of pseudopodium extension, whereas the second redirects the actin cytoskeleton polymerization machinery to the edge opposite to the stressed side of the cell.

Movies available online

Key words: Motility, Hydrodynamic flow, Mechanosensitivity, *Dictyostelium discoideum*

Introduction

In addition to specialized cell types such as hair cells, many eukaryotic cells exhibit force sensitivity, especially in the context of cell adhesion. For instance, fibroblasts adhere to the extracellular matrix through focal contact areas, whose number and surface increase with the mechanical tension applied to the cell (Choquet et al., 1997; Riveline et al., 2001). The direction of actin stress fibers is then clearly in continuity with the disposition of the extracellular fibrillar material (Zamir and Geiger, 2001). Epithelial cells form closed vessels through the apposition of membranes bearing homotypic adhesion proteins. The expression of genes involved in the stability of these structures is induced by the blood flow shear stress (Chappell et al., 1998; Nerem et al., 1998). Keratinocyte fragments moves upon mechanical stimulation (Verkhovsky et al., 1999). The mechanosensitivity seems to have evolved from mechanisms of cell osmotic protection, because stress-activated membrane channels exists in all organisms from bacteria to humans (Hamill and Martinac, 2001).

In this work, we present another example of a cellular response to force: shear-flow-induced cell motility (SFICM) of *Dictyostelium discoideum*. This simple eukaryote is a genetically and biochemically tractable model organism that is used extensively to study cytoskeleton organization, chemotaxis, cell differentiation and development (Kay, 2002). The lifestyle of *D. discoideum* consists of two phases. During the vegetative phase, cells feed by phagocytosis of bacteria and yeast cells, and exhibit random explorative motility as well as chemotaxis toward folate, a molecule produced by most prokaryotes. Upon starvation, *D. discoideum* cells aggregate, secreting 3′-5′-cyclic AMP (cAMP) to attract other cells by chemotaxis. The pseudoplasmodium then undergoes a developmental process coordinated by the secretion of several diffusible molecules such as cAMP, ammonia and DIF (a chlorinated alkylphenone). Individual cell movements within the cell mass are defined by these gradients and by local cell contacts (Weijer, 1999).

The directed movement of cells during chemotaxis has been the subject of many studies (Iijima et al., 2002). It consists of several phases. First, the cell detects a gradient of a chemoattractant molecule, either spatial or temporal, by binding to specific receptors. The amplification of the external signal perceived results in the building up of an intracellular gradient of a specific molecule, which defines two edges in the cell (polarization). The localized polymerization of actin at the front edge leads to the protrusion of the membrane surface, which increases the cell surface contact area (pseudopod) (Theriot and Mitchison, 1991). This is followed by myosin-II mediated contraction of the rear edge of the cell (Jay et al., 1995). At the molecular level, two molecules have been shown to play the role of a polarized second messenger: phosphatidyl inositol (3,4,5)-trisphosphate [PtdIns(3,4,5)P_3] and PtdIns-

(3,4)-bisphosphate [PtdIns(3,4)P_2]. These lipids recruit the actin-nucleating factor WASP/Scar, which drives the formation of an active Arp2/3 complex and initiates the barbed-end growth of actin filaments. Pseudopodium extension is therefore subordinated to the production of these lipids. Myosin-II activation proceeds by a cascade of phosphorylations involving the myosin II heavy chain kinase A (MHCKA) and the p21 activated kinases (PAKs) (Chung and Firtel, 1999). Although the molecular details of myosin-II recruitment and specific localization at the plasma membrane are unknown, it has been established that a peak of cGMP production follows cell stimulation, which controls myosin II association with the actin cytoskeleton (Newell, 1995). Both actin polymerization and myosin activation are under the control of small GTP-binding proteins of the Ras or Rac subfamilies, whose GTPase activity set the pace of the cell response (Chung et al., 2000).

We previously used shear-flow-induced cell detachment to quantify *D. discoideum* adhesion to substrate (Decave et al., 2002b). For a given cell, detachment occurs for values of the applied hydrodynamic stress above a threshold. Statistically, cell detachment follows apparent first-order kinetics. The threshold stress depends on cell size, the nature of the substrate and the presence of adhesion proteins at the plasma membrane surface (Cornillon et al., 2000) but, to first approximation, is not affected by depolymerization of the actin or tubulin cytoskeleton. By contrast, the detachment rate constant is strongly affected by the presence of an intact actin cytoskeleton and by the cell-substrate adhesion energy. Part of these results was interpreted within an adhesive belt model describing the passive behavior of the cell edge under external or internal forces (Garrivier et al., 2002). This model predicts that, below a threshold, the cell edge will not move and that, above it, the membrane will be peeled of the substrate at a constant velocity. However, this model could not unambiguously interpret the effect of actin microfilament depolymerization, which accelerates cell detachment kinetics tenfold. Cells were therefore visualized under shear flow to understand how microfilaments delay cell detachment. Here, we show that shear flow induces an active cell response, resulting in the reconstitution of cell-substrate contact area and cell motility. The speed of this movement is limited by membrane peeling at the rear cell edge (Decave et al., 2002a). In addition, we demonstrate that the origin of cell movement lies in internal forces. This study gives insights into the complex bidirectional network linking cell mechanics to cell signaling pathways (Asthagiri and Lauffenburger, 2000; Ingber, 1997).

Materials and Methods

Cell preparation and chemicals

Ax-2 cells were grown at 22°C in axenic medium (Watts and Ashworth, 1970) in shaking suspensions (180 rpm). The WF1 plasmid allowing in vivo expression of the PH domain-containing *Dictyostelium* protein CRAC (cytosolic regulator of adenyl cyclase) coupled to GFP (Parent et al., 1998) was kindly provided by P. Devreotes (Johns Hopkins University, Baltimore, MD) and electroporated into Ax-2 cells essentially as described (Cornillon et al., 2000). CRAC-GFP-expressing cells were selected with 20 μg ml^{-1} G418 (Roche Diagnostic, Meylan, France). Vegetative cells were harvested during exponential growth phase at a density of 2×10^6-4×10^6 cells ml^{-1}, pelleted by centrifugation (1000 ***g***, 4°C, 4 minutes), washed twice in Sörensen phosphate buffer (2 mM Na_2HPO_4, 14.5 mM KH_2PO_4, pH 6.2) and used immediately. *N*-(3-chlorophenyl)-isopropyl-carbamate (CIPC), nocodazole, cytochalasin A, LY294002 and wortmannin were supplied by Sigma (St Louis, MO, USA), and dissolved in DMSO.

Experimental setup

A transparent lateral flow chamber was built that consisted of a Lucite top part, a 0.25 mm thick Teflon gasket delimiting the flow chamber, a microscope glass plate and a Lucite bottom part, assembled with four screws (Fig. 1). Before use, microscope glass slides (Erie Scientific, Portsmouth, NH, USA) were cleaned with a mild detergent, etched for 5 minutes in a 14.5 M NaOH solution, thoroughly rinsed with distilled water, dried under a dust-free pressurized air flow and stored in a dessicator. The flow chamber was connected to large upper and lower tanks, both filled with Sörensen phosphate buffer. Fluid flowed by gravity, at a rate controlled by the height between its levels in the tanks. The flow rate was deduced from the volume transferred during the experiment.

Cells were resuspended in Sörensen phosphate buffer at a density of 10^6 cells ml^{-1}, introduced into the flow chamber through a three-way stopcock and allowed to settle for 1 minute. The surface density was ~100 cells mm^{-2}, corresponding to <1% surface coverage. No hydrodynamic interaction between adjacent cells was detected during the experiments. Cells contained in the inlet tubing were then washed out at low flow rate (1 ml min^{-1}, corresponding to a shear stress σ=0.12 Pa) for 2-3 minutes. Image acquisition was started and, at a predefined time, a larger steady flow rate (7.5-58 ml min^{-1}, σ=0.85-6.2 Pa) was applied and maintained until the end of the recording. In experiments involving drugs for cytoskeleton depolymerization or phosphoinositide 3-kinase (PI3K) inhibition, the cell pellet was directly resuspended in Sörensen phosphate buffer containing the drug and the fluid used for the flow experiment also contained the drug at the same concentration.

The action of shear flow on cells adhering to the substrate is determined by the hydrodynamic forces exerted on the cell. Because the Reynold's number is low (<100), inertial effects can be neglected. Considering cells as an elastic solid, the net force and torque exerted by the flow on an adhering cell are proportional to the wall shear stress σ. In this geometry,

$$\sigma = \frac{6D\eta}{le^2}, \quad (1)$$

where D is the flow rate, η the dynamic viscosity of the fluid, e the distance between the top and the glass plate, and l the width of the flow chamber.

The critical shear stress for cell detachment $\sigma_{1/2}$ is 2.6 Pa for *D. discoideum* cells on glass (Decave et al., 2002b). At the highest stresses tested, an increasing cell fraction detached during the experiment. In order to measure flow-induced cell motility and not cell peeling, cells that detached during the first 3 minutes following the onset of the flow were not included in quantitative cell motility measurements.

Data acquisition

Flow-induced cell motility was studied by recording the individual large-scale motions of about 200 cells. A 2×2.5 mm^2 area was examined on the flow chamber glass plate at low magnification (2.5×) under dark-field illumination in a ICM405 inverted microscope (Zeiss, Germany) with a CCD camera (SP-Eye; Photonic Science, UK) interfaced to a computer. The sampling rate was adjusted to the speed of cell movements. Typically, a sequence of 20 images was recorded, each separated by 30 seconds, using Image-Pro Plus software (Media Cybernetics, MD, USA). Flow was applied 10 seconds after the first image. The individual centroid motion of 32 randomly selected cells was reconstructed, using a slightly modified version of the

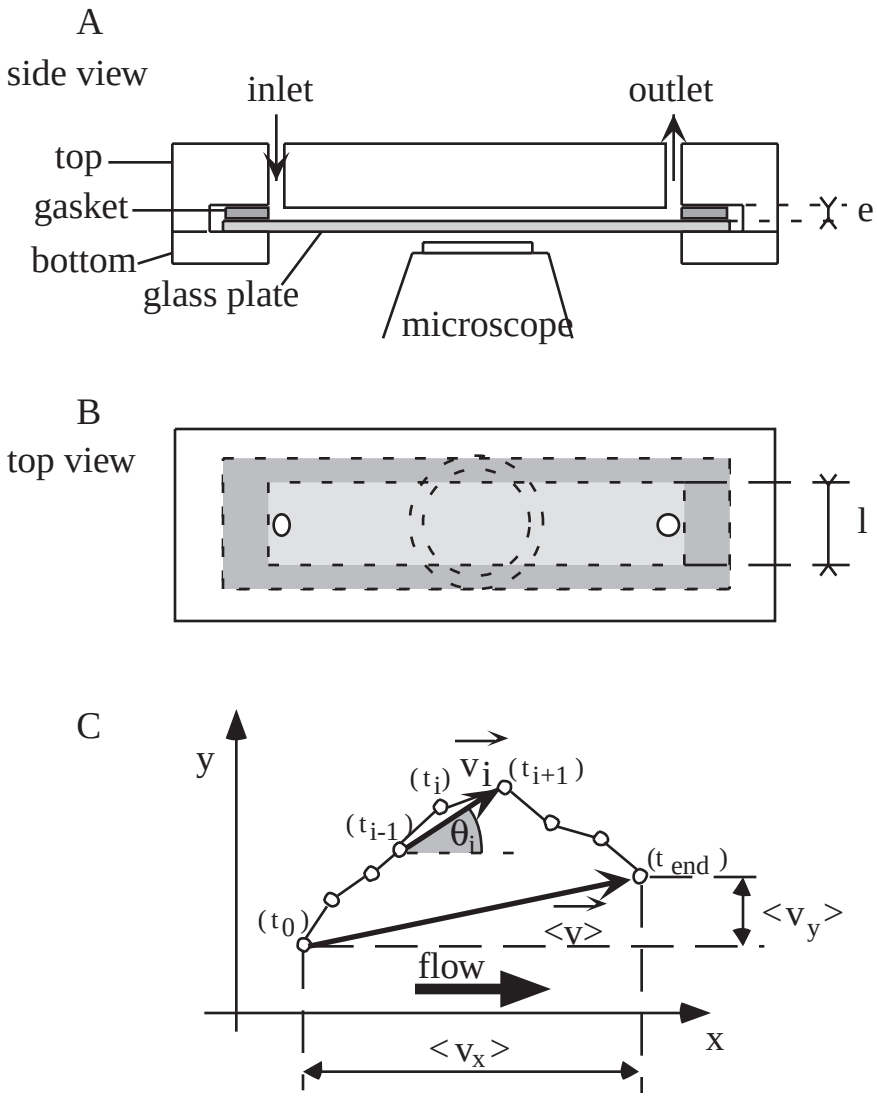

Fig. 1. Experimental setup. (A) A uniform hydrodynamic flow was generated between the lucite top part and the microscope glass plate on which cells adhere. Cell movements were imaged by an inverted microscope under various illumination types and recorded by a digital camera coupled to a computer. (B) The hydrodynamic shear stress applied to the cells is related to the chamber width l and height e and to flow rate D through Eqn 1 (see Materials and Methods). (C) Representation of cell movements. The cell position is represented as successive points in Cartesian coordinates, where the x axis denotes the direction of the flow. The translational cell velocity during a track $<\vec{v}>$ is defined by Eqn 3 from the cell positions at the initial time (t_0) and the last cell position recorded (t_{end}). The projections of the translational cell velocity over the directions parallel and perpendicular to the flow are denoted $<v_x>$ and $<v_y>$. The instant cell velocity $\vec{v}(t_i)$ is calculated according to Eqn 2 from the cell positions at the previous (t_{i-1}) and following (t_{i+1}) instant times and given in orthoradial coordinates, where θ_i is the angle between the speed and the flow.

'Manual-tracking' Image-Pro Plus macro (freely available at http://www.solutions-zone.com/). Briefly, at a given time, a small area of interest was defined around a given cell, the image was segmented to detect cell contours and the centroid position was calculated. This semiautomatic procedure was repeated for each time frame and the results were reported in an Excel datasheet. The position of the observed area in the flow chamber did not affect the results.

In order to determine the pseudopodium emission frequency, cells were observed at a 20× magnification under phase-contrast illumination. In this case, a sequence of 40 images was recorded at a 1 Hz sampling rate and the flow started immediately after the fifth image. The experiment was reproduced several times in order to collect enough data for statistical treatment (typically, 30 cells).

The deformation of cell-substrate contact area during flow-induced motility was recorded on single cells observed at a 40× magnification under reflection contrast interference microscopy (RICM) using a Zeiss ICM405 inverted microscope with a modified epifluorescence illumination pathway using optical components purchased from Melles-Griot (Carlsbad, CA, USA) (Bereiter-Hahn and Vesely, 1995). Monochromatic light at 546±10 nm was selected using a set of band-pass and interference filters, and linearly polarized by inserting a plate polarizer in the excitation beam. A (50:50) beam splitter was placed in the dichroic mirror lodging. A one-quarter-wavelength plate (137 nm) was put between the 40× long-range microscope objective and the flow chamber glass plate, and an analyser (Polaroid polarizer) was inserted in the emission pathway of the microscope. Sequences of 40-60 images were recorded at a 0.25-0.5 Hz sampling rate, starting 15 seconds after application of the flow. Linear post-recording image processing was applied to improve image quality.

CRAC-GFP-expressing cells were imaged under shear flow or without shear stress at a 60× magnification under epifluorescence illumination in an Olympus IX-70 inverted microscope (Olympus, France) with an intensified CCD camera (ISIS-3; Photonic Science, UK) interfaced to a computer. Fluorescent cells were randomly selected and the intracellular CRAC-GFP profile quantitatively evaluated using Image-Pro Plus software. Cells exhibiting a clear enrichment in CRAC-GFP on the edge of the cell (>50% increase above mean intracellular level) were considered as polarized and the CRAC-GFP distribution was further analysed for its orientation.

Quantitative analysis of cell motility

Individual cell tracks consist in series of points (centroid position), originating at the position recorded on the first frame. The instant cell velocity is calculated according to the following formula:

$$\vec{v}(t_i) = \frac{\vec{x}(t_{i+1}) - \vec{x}(t_{i-1})}{t_{i+1} - t_{i-1}}, \qquad (2)$$

where $\vec{x}(t_i)$ designates the position of the cell in the ith frame at time t_i. The velocity vector is expressed in orthoradial coordinates with respect to the flow. Individual cell motion is described by the plot of the velocity modulus v_i and its angle θ_i with respect to flow as a function of time t_i. The statistics of cell motion are described by constructing a histogram of the velocity modulus and its angle with respect to flow, using data from 20 or 32 individual tracks. Directionality is defined as cosine θ_i, averaged over all centroid movements $<\cos\theta_i>$. Cells moving randomly have a directionality of 0, whereas cells moving straight in the direction of the flow have

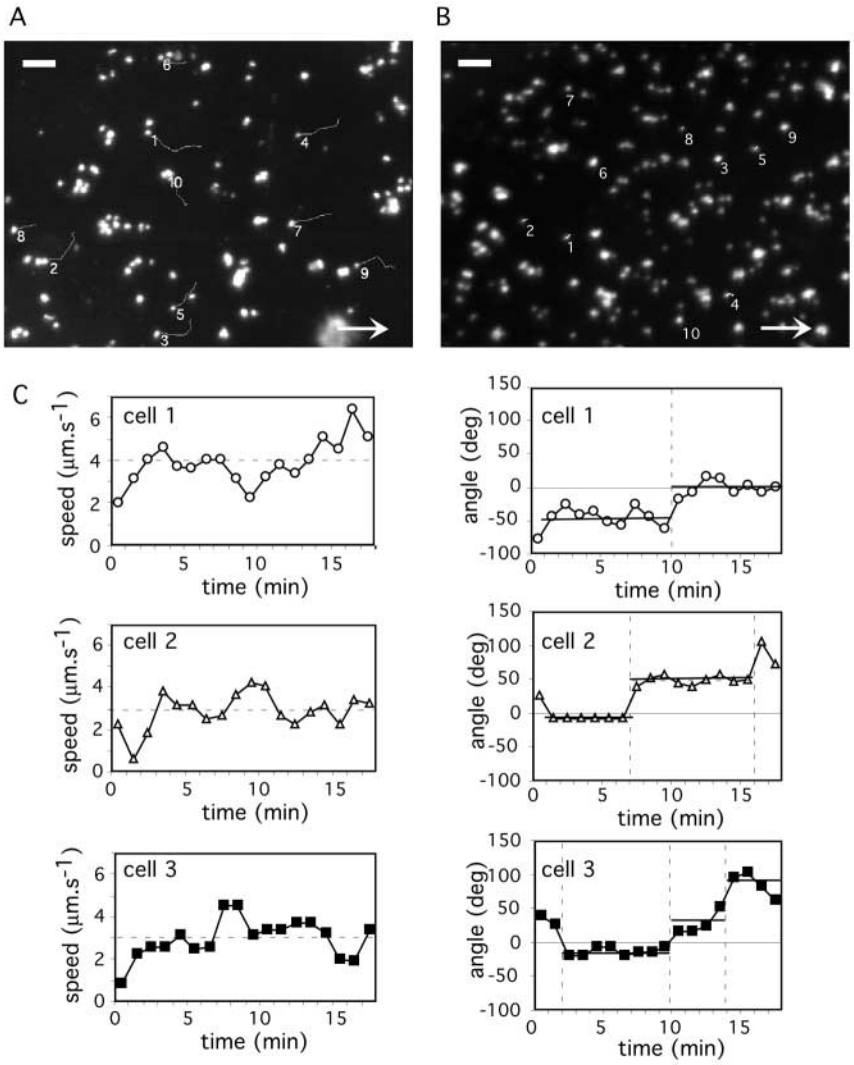

Fig. 2. Shear flow-induced cell motility. Cells were submitted to a 1 Pa shear stress and monitored under dark field illumination at a 2.5× magnification for 10 minutes. A set of representative cell tracks is shown superimposed over the first image recorded. Each track starts on the cell identified by the indicated number and ends at the free end of the line. Scale bar, 100 μm. Arrow points into the flow direction. (A) Untreated cells. These data correspond to Movie 1. (B) In the presence of 20 μg ml^{-1} CIPC. These data correspond to Movie 2. (C) Example of individual cell track analysis. The instant velocity and angle with respect to flow of the cells denoted 1, 2 and 3 in (A) were calculated according to Eqn 2 and represented in orthoradial coordinates. Left: speed modulus as a function of time. The dotted lines indicate the average speed modulus. Right: speed angle as a function of time. The solid lines represent portions of straight-line movements. The dotted lines indicate cell turns.

a directionality of 1. Persistence is the average time during which cell centroids follow linear paths, whatever their directions, at a ±22.5° angle. The inverse of the persistence is the turning frequency.

For a given cell, the translational velocity is defined as the average velocity during the 10 minutes of recording is defined as

$$\langle \vec{v} \rangle = \frac{\vec{x}(t_{end}) - \vec{x}(t_0)}{t_{end}}, \quad (3)$$

where t_{end} is the time at the end of the recording or when the cell detaches. The translational velocity is also obtained by averaging over 20 or 32 cells. This velocity is expressed in Cartesian coordinates, where x designates the direction of the flow and y the direction perpendicular to this (Fig. 1). The proportion of responding cells is defined by segmenting the images using the Image-Pro Plus software and counting the number of cells whose final position (at t_{end}) does not overlap with the initial one (at t_0).

The pseudopodium emission frequency is determined by the following procedure. For each cell, a pseudopodium was detected when a dark 2-3 μm wide area appeared on the side of the cell and lengthened about 2 μm during the following 3-4 seconds. One pseudopodium emission event was then scored at the time when the protrusion appeared. As a result of this procedure, no pseudopodium was counted in the first frame (time 0). The same analysis was performed on 30 cells. At a given time, the pseudopodium emission frequency is therefore given by the total number of pseudopodia detected divided by the cell number.

For cell-substrate contact area recordings, the motions of the front and the rear edges were defined by the following procedure. First, individual images are segmented and the center of mass of the cell-substrate contact area determined using the Image-Pro Plus software. The overall direction of cell movement is then determined by fitting the motion of the center of mass of the contact area with a straight line. The positions of the front and rear edges are obtained on each image by the extreme extension of the cell along the direction of the movement. The projections of the front and rear edges on the straight line are finally plotted as a function of time.

For CRAC-GFP cells, the degree of orientation of the internal polarization gradient with respect to the flow is evaluated and the cells grouped into four classes as follows. For each cell, the direction of the CRAC-GFP gradient is determined by searching for the line passing through the center of mass that gave the steepest fluorescence intensity profile. In this search, the CRAC-GFP enrichment seen in nascent endosomes is avoided. Some cells presented multiple fluorescence fronts and are therefore scored accordingly. Cells whose intracellular CRAC-GFP gradient is oriented in the direction or opposite to the flow (within ±70°) are scored as 'co-linear' or 'reverse'. The remaining cells, where the direction of the gradient is at right angle (within ±20°) to the flow, are scored as 'perpendicular'.

Results

Passive and active behavior of adherent *D. discoideum* cells under hydrodynamic flow

D. discoideum cells adsorbed on glass were exposed to an uniform hydrodynamic flow and observed continuously for 10 minutes. As shown in Fig. 2A, Movie 1 (see http://jcs.biologists.org/supplemental/) and Table 1, the vast majority of the cells exhibits a net movement in the direction of the flow. In addition, depending on shear stress value, a certain proportion of the cells detach from the plate and are taken away in the bulk flow, as previously reported (Decave

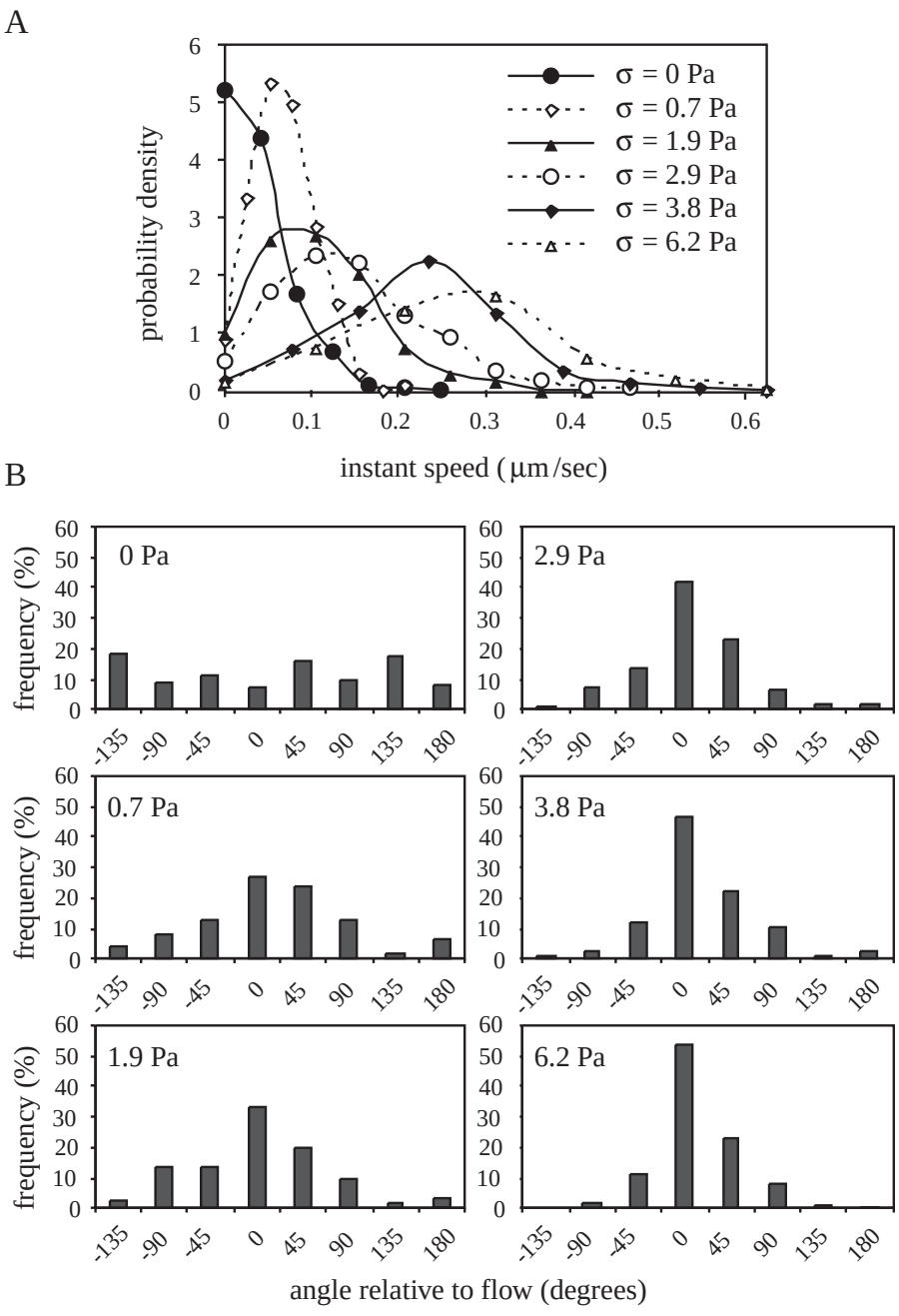

Fig. 3. Kinematic analysis of shear flow induced cell motility. Cell motions were recorded under application of the indicated shear flow. Individual cell tracks are analysed as a set of instant velocity between successive time frames according to Eqn 2.
(A) Probability distribution of speed modulus. The distribution of speed modulus was normalized so that the area under each curve is 1. (B) Angular distribution of cell instant velocities with respect to the flow axis. Directions of cell movement were decomposed into eight 45° classes, centered on the eight directions indicated.

et al., 2002b). By contrast, cell movement occurs randomly in the absence of flow (Table 1). When the flow is reversed, cells respond almost instantaneously and move in the opposite direction (data not shown). In order to study this SFICM in a quantitative manner, the individual motions of 20 or 32 cells were tracked and the instant velocities of individual cells and their distribution over the population were quantified.

Fig. 2C shows a set of representative cell tracks, expressing instant velocities in orthoradial coordinates with respect to the flow. The movement of most cells consists of straight-line portions, most of which are aligned along the flow. The turning frequency is independent of shear stress (Table 1). These features are qualitatively comparable to the random motion of *D. discoideum* cells on solid surfaces or to their behavior upon chemotactic stimulation (Killirch et al., 1993; Vicker, 1994) but differ in their speed and polarity.

The speed of cell movement increases with shear stress in a non-linear manner (Fig. 3A, Table 1). For large flow rates (σ=6.2 Pa), cell detachment predominates over cell motility, complicating precise cell speed measurements. Cells were classified into two groups, according to the duration of their tracks. Cells that detach rapidly (<60 seconds, 80% of cells) moved faster ($\langle v \rangle$=0.42±0.1 μm second^{-1}, 20 cells) than cells that stay longer on the glass plate ($\langle v \rangle$=0.22±0.8 μm second^{-1}, 20 cells). Fig. 3A shows cells from the second group only. Instant velocities over 0.5 μm second^{-1} are therefore easily observed (50 times larger than the average speed of unstimulated cells). At zero force, cell movement is obviously random, but cells submitted to shear stresses as low as 0.8 Pa already show clear polarization (Fig. 3B). At 2.9 Pa, 80% of cell movements are constrained in a 50° cone. The directionality of cell movement, defined as the average value of the cosine of the cell speed angle with respect to flow $\langle \cos\theta_i \rangle$, therefore increases with shear stress (Table 1).

Is cytoskeleton dynamics involved in SFICM? Because *D. discoideum* possesses both microfilaments and microtubules, we tested the effect of cytochalasin A, a selective actin depolymerization drug (Condeelis et al., 1988). Addition of 1 μg ml^{-1} cytochalasin A, a concentration sufficient to eliminate most microfilaments, decreases $\langle v_x \rangle$ (the projection of the translational velocity in the flow direction) from 0.6±0.2 μm second^{-1} to 0.02 μm second^{-1}. SFICM therefore involves active actin polymerization. Similarly, SFICM is also abolished by 20 μg ml^{-1} CIPC, a carbamate herbicide that affects both cytoskeleton networks (Oliver et al., 1978) (Fig. 2B, Movie 2). Staining of fixed cells with fluorescently labeled phalloidin shows a clear reduction of filamentous actin in CIPC-treated cells (not shown). The effect of CIPC on cell motility is very fast (<30 seconds) and, on the short term, reversible (~1

Table 1. Kinematics of *D. discoideum* SFICM

Shear stress (Pa)	Number of cells analyzed	% of responsive cells	Directionality $\langle\cos\theta_i\rangle$	Turning frequency	$\langle v_x\rangle$ (μm/s)	$\langle v_i\rangle$ (μm/s)
0	32		–0.07	0.078	–0.005±0.001	0.05±0.03
0,72	32	65	0.47	0.063	0.016±0.001	0.058±0.03
1,92	20	89	0.53	0.074	0.047±0.025	0.092±0.06
2,94	20	82	0.68	0.058	0.092±0.052	0.13±0.02
3,84	32	83	0.71	0.071	0.14±0.04	0.19±0.04
7,2	20	87	0.79	0.062	0.19±0.03	0.22±0.07

D. discoideum cells were submitted to the indicated shear flow and individual cell tracks were recorded and analyzed to determine the kinematics parameters as described in Materials and Methods and Fig 1. $\langle v_x\rangle$ is the average speed of the cells in the direction of the flow (Eqn 3) and $\langle v_i\rangle$ is the average modulus of instant cell velocities (Eqn 2).

minute). We previously showed that the rate of shear-flow-induced cell detachment is increased tenfold in the presence of CIPC, whereas the efficiency of cell detachment is unaffected (Decave et al., 2002b). Microscopic observation of CIPC-treated cells confirms these results and also shows that, in the presence of CIPC, cells detach without previous displacement on the substrate; by contrast, in its absence, cell move over tens of micrometers before leaving (Fig. 2A,B, Movies 1, 2). This points out a clear difference between active and passive behavior of *D. discoideum* cells under shear flow. Passive behavior occurs when the actin cytoskeleton is depolymerized, in which case cell detachment corresponds to a transition between immobility and peeling. Active behavior requires the presence of an intact actin cytoskeleton, and cell detachment corresponds then to a transition between SFICM and peeling.

Evolution of cell-surface contact area during flow-induced motility

To gain insight into the origin of SFICM, we observed cells at a higher magnification under the RICM technique, to image the cell-substrate contact area. Dark regions correspond to zones in which the membrane of the cell lies within 100 nm of the substrate (Bereiter-Hahn and Vesely, 1995). Vegetative *D. discoideum* cells usually present a single large contact area, whereas developing cells have several smaller ones (Weber et al., 1995). Fig. 4 shows the evolution of the contact area for single cells submitted to a 4 Pa hydrodynamic shear stress, in the absence or in the presence of CIPC (Fig. 4A,B). Qualitatively, cells move thanks to local increases of their contact area on the edge opposite to the flow and retraction of the edge facing the flow. Cells deprived of active actin cytoskeleton are peeled off the substrate at the same rate but obviously lack the ability to reconstitute the contact area. Notably, for shear stresses below the threshold $\sigma_{1/2}$=2.6 Pa determined for cell detachment from glass (Decave et al., 2002b), no change in the cell contact area can be seen in the presence of CIPC on the experimental time scale (data not shown). To put these observations on a more quantitative basis, we measured the movement of the rear and front edges of the cell contact area. These points are defined as the extreme extensions of the cell contact area in the direction of the movement. This is shown in Fig. 4C,D for control or CIPC-treated cells, respectively (for a shear stress σ=4 Pa). The movement of both ends of the cell is strikingly different. The rear edge of the cell moves steadily, whatever the state of the actin cytoskeleton, defining a constant peeling velocity. However, the front edge of control cells presents alternate phases of immobility and of rapid forward bursts of movement (marked by arrows; see also the sequence 160-172 seconds in Fig. 4A). The front edge is immobile in the presence of an actin-depolymerizing drug. Plotting the frequency histograms of the instant velocity of both edges (Fig. 4E,F) provides the characteristics of their movement. At a 4 Pa applied shear stress, the rear peeling velocity is 0.17±0.02 μm second^{-1}, the frequency of front edge bursts is 0.05±0.01 Hz, the burst growth rate is at least 0.4±0.1 μm second^{-1} and the length of each burst is 1.9±0.2 μm. In addition, each burst increases cell contact area by ~20 μm^2.

These results fully confirm the observations made at a lower magnification. Thus, SFICM involves two phenomena: shear-stress-induced peeling of the cell rear edge and periodic restoration of intimate cell-substrate contact area at the front edge. The restoration phase is rapid (<4 seconds) and corresponds to a 2 μm extension in the direction of the flow. A remarkable feature of SFICM is that it is in continuity with spontaneous cell movements that are actually detectable at shear stress values fivefold lower than the threshold for cell detachment.

Cells respond to increasing forces by adjusting pseudopodia emission frequency

As shown above, the speed of cells performing SFICM increases with shear stress (Fig. 3A). This speed is that of the cell mass center, averaged over 20 second time intervals. How do the cell edges respond to different shear stress values? The deformation of cell contact area was studied for three values of the applied shear flow (Fig. 5). The kinematic parameters of the rear and front edges are given in Table 2. The rear edge velocity increases non-linearly with applied shear stress. As for

Table 2. Analysis of cell edge movements under shear flow

	σ=1.8 Pa	σ=3 Pa	σ=4 Pa
Rear peeling velocity (μm/s)	0.045	0.11	0.17
Front edge velocity (μm/s)	0.040	0.12	0.16
Burst length (μm)	1.88	1.72	1.89
Burst growth rate (μm/s)	0.45	0.34	0.40
Burst frequency (Hz)	0.01	0.06	0.05

The table summarizes the analysis of the front and rear cell edge movement induced by the flow as shown in Fig. 5. The peeling (rear edge) velocity, the front edge velocity, the length of and growth rate of the burst extensions, and their emission frequency were determined at three shear stress values. Data are representative of several experiments.

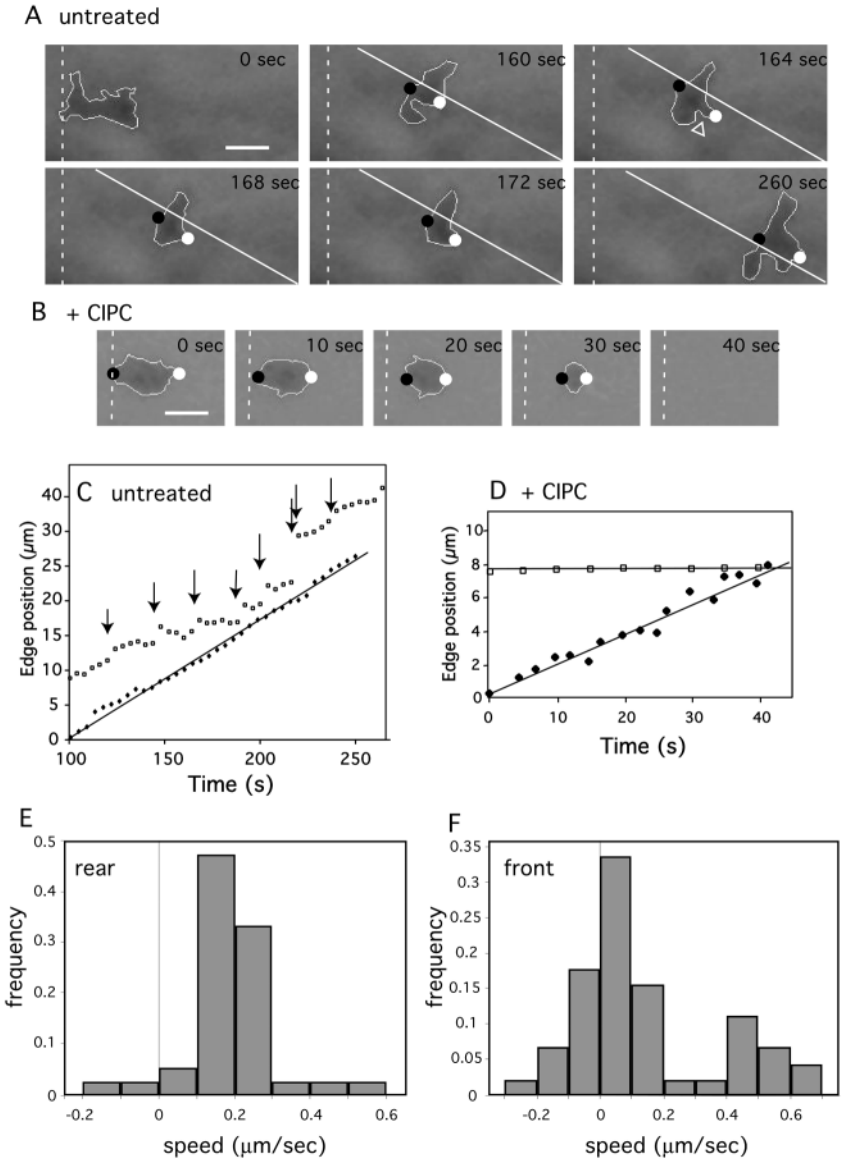

Fig. 4. Flow-induced evolution of cell-substrate contact areas. Individual cell-substrate contact area was imaged during shear flow application (σ=4 Pa) by RICM at a 40× magnification. The peeling velocity has already been analysed for its relationship with the applied shear stress (Decave et al., 2002a). (A,B) Representative set of cell substrate contact area position over time. The dotted line indicates the position of the rear of the cell at the beginning of the recording. The cell's rear and front edges are indicated by black and white circles, respectively. Arrows indicate the flow direction. Arrowheads indicate rapid increases of cell-substrate contact area (bursts). (A) Untreated cells. The solid line indicates the overall direction of the cell during the considered straight movement. (B) In the presence of 20 μg ml^{-1} CIPC. (C,D) Positions of cell rear (closed diamonds) and front (open squares) edges over time for untreated (C) and CIPC-treated (D) cells. The data correspond to the cells shown in A and B, respectively. Arrows indicate rapid increases of cell-substrate contact area (burst phases). The sixth extension of the front edge (C, *t*=215 seconds) is longer than the others (7 μm instead of 2 μm). This corresponds to several bursts occurring simultaneously. Notice that the rear peeling velocities of CIPC-treated and untreated cells are identical in this case, in which both cells are going to detach. (E,F) Distribution of rear (E) and front (F) edge instant velocities. The data correspond to the cell shown in A. The cell rear movement exhibits a single peak at 0.2 μm second^{-1} velocity. Bursts and immobility phases in the cell front movement correspond to peaks at 0.5 μm second^{-1} and 0 μm second^{-1}, respectively.

the front edge, both the growth rate and length of the bursts are not affected by the applied stress, in contrast to the burst frequency, which clearly increases with applied stress between 1.8 Pa and 3 Pa, and saturates between 3 Pa and 4 Pa, indicating that an upper limit has been reached. Cells respond to increasing peeling velocity by increasing the frequency of the cell-substrate contact restoration mechanism. SFICM therefore proceeds through unitary cell-substrate area extensions of constant growth rate.

Because the restorative mechanism of cell-substrate contact area evidenced above involves actin polymerization, it is likely that burst phases seen by RICM are the traces of pseudopodia emitted in response to applied shear stress. In *D. discoideum*, pseudopodia are indeed producing propulsive forces as well as initiating cell contact area. The unitary size and growth rate of these bursts are similar to those of the pseudopodia produced during *D. discoideum* chemotaxis toward cAMP (Weber et al., 1995). We therefore looked at the frequency of pseudopodium emission in response to applied shear stress. *D. discoideum* cells were imaged at 1 Hz at a 20× magnification under phase-contrast illumination to visualize pseudopodia, which appear as dark protrusions on the side of the cells. Hydrodynamic flow was applied 5 seconds after having triggered image acquisition. The recordings were subsequently scanned to detect pseudopodia (see Materials and Methods) and the pseudopodium emission frequency was calculated and plotted as a function of time (Fig. 6A). In the absence of shear flow, the number of pseudopodia emitted per cell and per second is 0.11±0.01 (from –4 seconds to 0 seconds in Fig. 6A and data not shown). As shear flow is applied (1.8 Pa), the pseudopodium emission frequency increases fivefold within 2 seconds, then decreases to a constant level (0.15±0.02 Hz cell^{-1}) slightly above the initial value, with a characteristic time of 3 seconds (from +2 seconds to +7 seconds in Fig. 6A). Here, again, cell response to flow is highly polarized, with >50% of the pseudopodia emitted in the direction of the flow during the immediate and adapted phases (Fig. 6B, Movie 3). The pseudopodium emission frequency increases with the applied shear stress during both the immediate and the adapted phases (Table 3). This shows that the application of shear stress results in an increased production of pseudopodia at the side of the cell opposite the region of maximal stress. It is likely that pseudopodia and the burst increase in cell-substrate contact area are different facets of the same actin-driven phenomenon, resulting in SFICM. It should be realized that the steady cell velocity previously

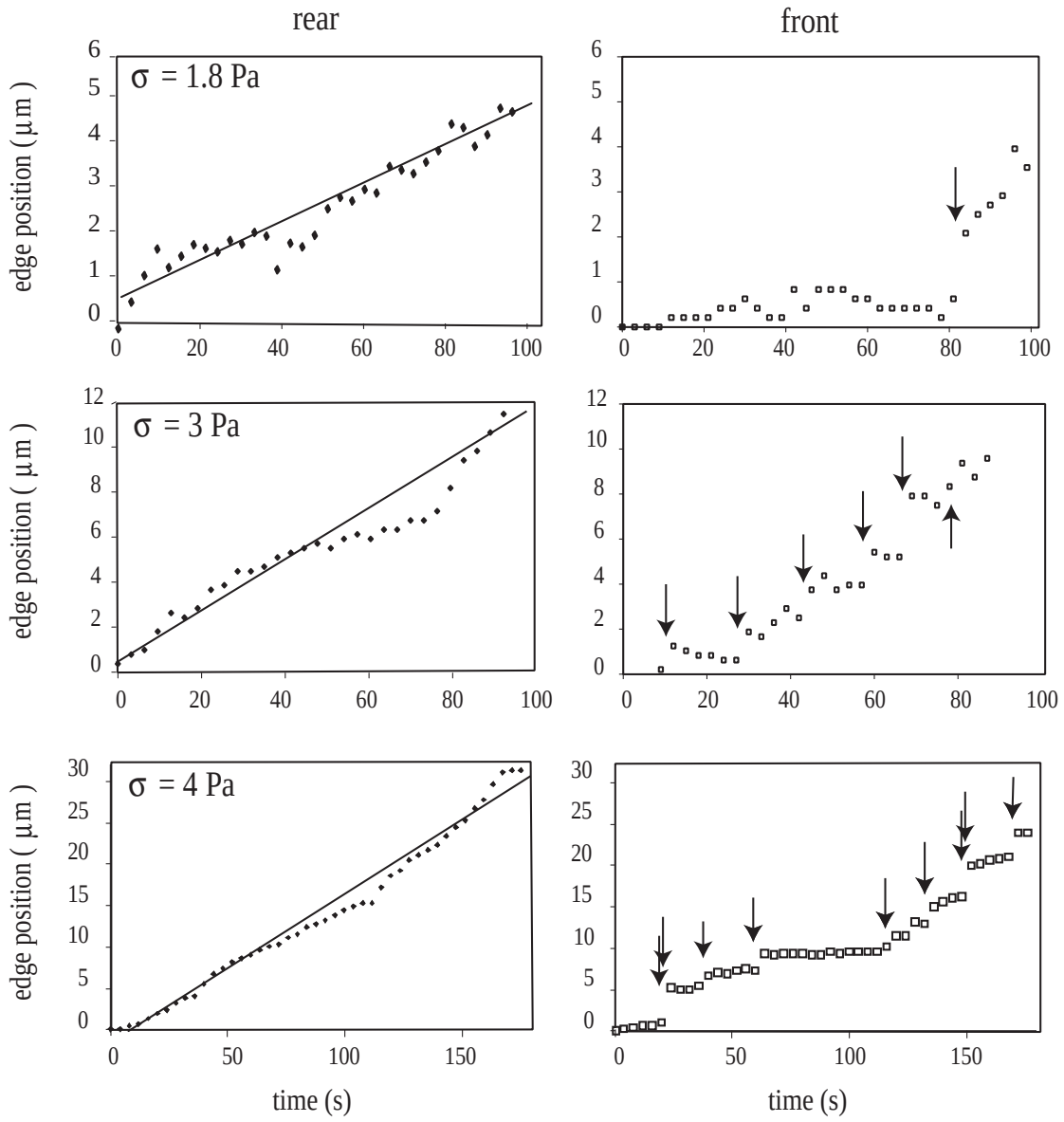

Fig. 5. During SFICM, cell speed is modulated by the frequency of fast increases in contact area (burst). Individual cell-substrate contact areas were imaged under SFICM at the indicated shear stress values by RICM at 40× magnification. The relative positions of cell rear (closed diamonds) and front (open squares) edges are plotted as a function of time. Arrows indicate the rapid increases in cell-substrate contact area (bursts).

measured corresponds to the adapted phase of the cell response to shear flow.

Proper localization of force-induced pseudopodia depends on PI3K activity

From the above results, it follows that SFICM corresponds to a polarized increase in pseudopodia emission in response to applied shear stress. Such cell motility clearly involves actin local polymerization mechanisms. The same cell molecular machinery is at work during chemotaxis. It has been shown that applying a chemoattractant gradient results in building up an internal gradient of phosphorylated phosphatidylinositol species such as PtdIns(3,4,5)P_3 (Chung et al., 2001). Key enzymes in the formation of such ‘internal compass’ include the PI3K family, which phosphorylates phosphatidylinositides at the third position in the inositol ring (Rickert et al., 2000). These enzymes are specifically inhibited by wortmannin or LY294002, which block ATP binding at the catalytic site (Vlahos et al., 1994). The PtdIns(3,4,5)P_3 gradient can be visualized using a CRAC-GFP fusion protein, which translocates at the plasma membrane upon stimulation of G-protein linked chemotatic systems (Parent et al., 1998). We therefore examined CRAC-GFP localization in cells submitted to constant shear flow (Fig. 7, Table 4).

Cells expressing CRAC-GFP exhibit one or several internal fluorescence fronts, even in the absence of shear flow (Table 4), corresponding to the pseudopodia emitted during random explorative movement of the cells on the substrate. Upon application of constant shear stress, a net reduction of the

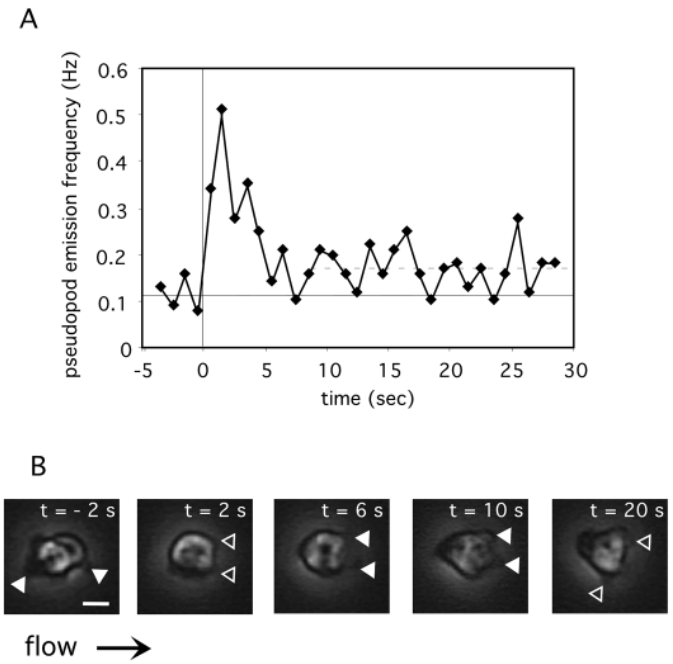

Fig. 6. Cells respond to increasing forces by an increased pseudopod frequency. *D. discoideum* cells adhering to glass were continuously monitored by phase-contrast microscopy. Cell response was triggered by application of a continuous 1.8 Pa shear stress (at t=0 seconds). Pseudopodia were detected by inspection over 50 cells as described under Methods and the pseudopodium emission frequency per cell was calculated at each time point. (A) Time course of cell pseudopodium emission frequency. The solid and dotted lines indicate the spontaneous and adapted pseudopodium emission frequencies, respectively. (B) A cell submitted to shear flow exhibiting nascent (empty triangles) and fully extended (filled triangles) pseudopodia, used in building up the curve shown in (A). The images are centered on the same cell and the indicated time is relative to the application of the flow. Different phases of cell response were selected: resting state (–2 seconds), onset of pseudopodium extension (+2 seconds), full immediate response (+6 seconds) and adapted phase (between +10 seconds and +30 seconds). Notice that most of the pseudopodia emitted after application of the flow protrude in the direction of the flow. Scale bar, 5 μm.

Table 3. Pseudopodia emission frequency under shear flow

	Immediate response	Adapted phase
σ=0.9 Pa	88	35
σ=1.8 Pa	228	54

The pseudopodia emission frequency was determined as in Fig. 6 at two shear stress values. The results are averaged over a 4 second time window. The table gives the percentage increase in pseudopodia emission frequency f during the immediate phase (0-4 seconds after flow application) and the adapted phase (8-12 seconds after flow application). The pseudopodia emission frequency of resting cells (f_0=0.11 Hz) is used as reference. The percentage increase is equal to $100(f–f_0)/f_0$.

number of cells showing multiple CRAC-GFP fronts is observed (from 40% to 16%), whereas 58% of the cells present a co-linear CRAC-GFP gradient. Examples of this fluorescent distribution are shown in Fig. 7. The phase-contrast images in the lower panel were taken 5 seconds after the fluorescence

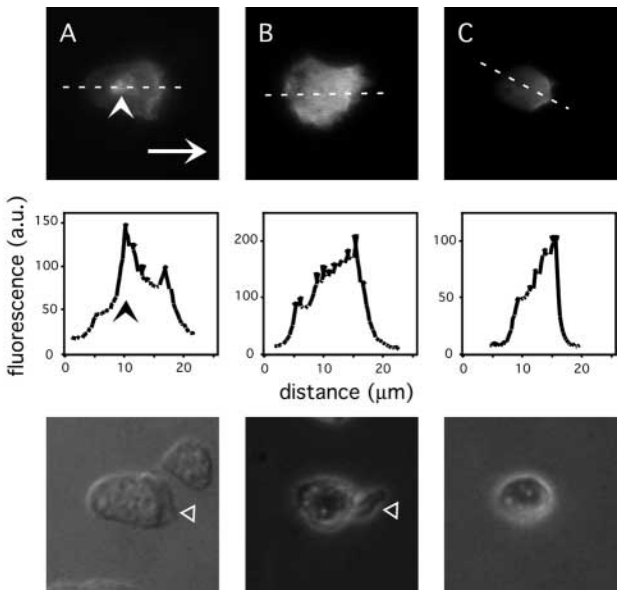

Fig. 7. Orientation of the internal PtdIns(3,4,5)P_3 gradient in response to shear flow. CRAC-GFP-expressing cells were observed at high magnification under constant shear flow (σ=2 Pa). Cells were observed between 2 minutes and 10 minutes upon application of the flow. The figure shows a gallery of cells presenting a unique CRAC-GFP front aligned with the direction of the flow (arrow). Statistics of the CRAC-GFP orientation is provided in Table 4. Top: GFP fluorescence. Middle: fluorescence intensity profile along the line shown in the top panel. Bottom: phase contrast images of the same cells. These images were taken 5 seconds after the fluorescence ones. The triangles point to membrane extensions that had occurred between the two pictures. In the fluorescence image of the cell reported in (A), an endocytic structure can be seen (arrowhead).

images of the upper panel. Membranes extensions at the PtdIns(3,4,5)P_3-rich edge, in the direction of the flow, are visible in Fig. 7A,B. The polarized pseudopodium emission therefore corresponds to the orientation of the internal PtdIns(3,4,5)P_3 gradient generated by the PI3K activity.

D. discoideum has three PI3K genes analogous to mammalian p110 PI3K: *DdPIK1*, *DdPIK2* and *DdPIK3* (Zhou et al., 1995). Null mutants lacking both *DdPIK1* and *DdPIK2* are severely deficient in chemotaxis and macropinosome formation, two processes involving plasma-membrane-driven actin polymerization. These phenotypes can be reproduced by treating wild-type cells with 0.2 μM wortmannin or 20 μM LY294002 (Buczynski et al., 1997; Rupper et al., 2001; Zhou et al., 1995). We therefore used these drugs to test the implication of PI3K activity in SFICM. Results are presented in Fig. 8 and discussed below for LY294002; wortmannin treatment gave similar results (not shown).

Fig. 8A shows a recording of *D. discoideum* cells performing SFICM in the presence of 30 μM LY294002 (Movie 4); the drug was added 5 minutes before triggering the flow. The movement of LY294002-treated cells is qualitatively similar to that of untreated ones, with long straight-line portions separated by sudden turns (turning frequencies are identical, data not shown). However, compared with untreated cells (Fig. 2A, Movie 1), the orientation of the movement is random, although cell speed along the trajectories is as high. This is confirmed by the kinematic analysis of cell movements

Table 4. Orientation of the CRAC-GFP front with respect to the flow

	Number of cells examined	CRAC front orientation with respect to the x-axis			Cells with multiple fronts
		Co-linear	Reverse	Perpendicular	
No stress	38	9	7	7	15
σ=2 Pa	31	18	4	4	5

CRAC-GFP-expressing cells were observed as shown in Fig. 8, either in the absence of flow (no stress) or in the presence of constant shear stress (σ=2 Pa). Individual cells presenting one or multiple clear CRAC-GFP fronts were imaged. The orientation of the CRAC-GFP fronts is compared with the direction of the x-axis, which corresponded to the direction of the flow when shear stress was applied.

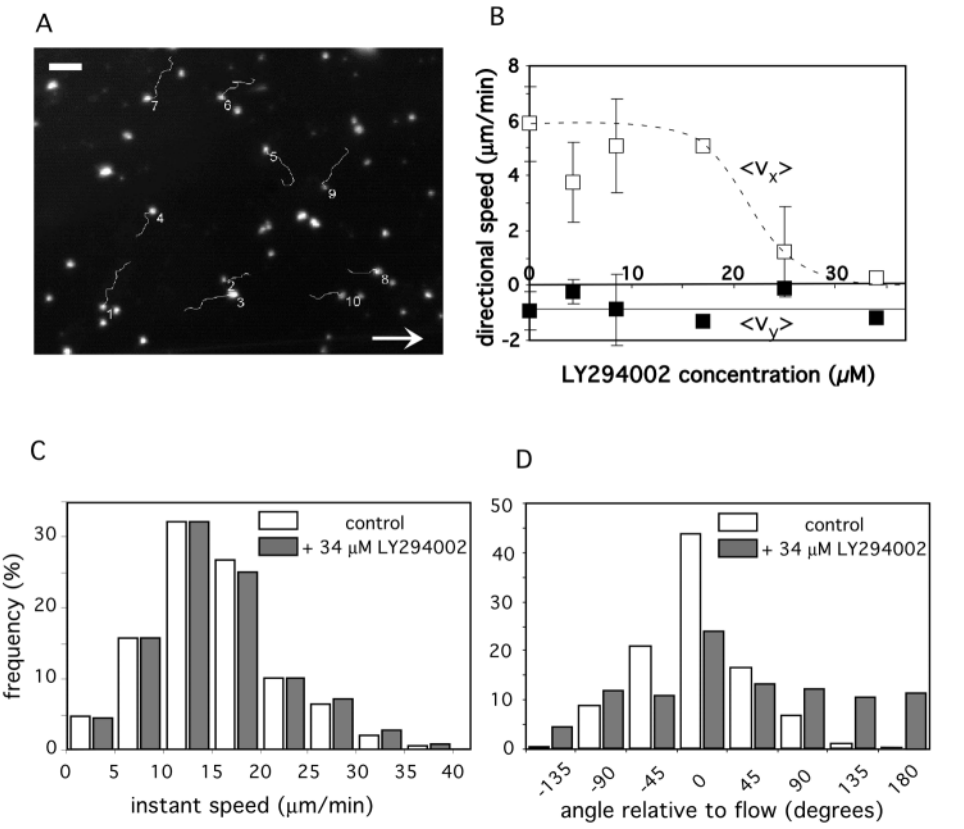

Fig. 8. Effect of PI3K inhibition on SFICM. (A) Cells were submitted to a 1.8 Pa shear stress in the presence of 34 μM LY294002 and monitored for 10 minutes under dark field illumination at a 2.5× magnification. A set of representative cell tracks is shown superimposed over the first image recorded. These data correspond to Movie 4. Each track starts on the cell near the corresponding number and ends up at the free end of the line. Scale bar, 100 μm. (B) Cells were submitted to a 1.8 Pa shear stress in the presence of the indicated LY294002 concentration and monitored for 10 minutes as in (A). The orthogonal projections of the average translational cell velocity over 10 minutes ($<v_x>$ and ($<v_y>$) were determined using Eqn 2 and plotted as a function of LY294002 concentration. (C) Distributions of instant cell velocity modulus in the presence (gray bars) or the absence (white bars) of 34 μM LY294002. Applied shear stress is 1.8 Pa. Data are from Fig. 2A and Fig. 8A. (D) Angular distributions of cell instant velocities with respect to the flow axis in the presence (gray bars) or the absence (white bars) of 34 μM LY294002. The histogram of the directions of cell movement is represented as in Fig. 3C. Applied shear stress is 1.8 Pa. Data are from Fig. 2A and Fig. 8A.

(Fig. 8C,D). The angle distribution of the instant velocity with respect to the flow is almost completely depolarized in the presence of the drug (directionality $<\cos\theta_i>=0.19$). By contrast, the modulus distribution of the instant velocity is unaffected. We thus concluded that inhibition of PI3K activity almost abolishes cell motion directionality without affecting its speed. Finally, a dose-response curve was constructed, using the orthogonal projections of the translational velocity to monitor the directness of the movement (Fig. 8B). Net movement in the direction of the flow (*x* axis: $<v_x>$) is abolished for LY294002 concentrations above 20 μM.

From these results, two important conclusions can be drawn. First, Fig. 8A and Movie 4 show clearly that many cells can move against the flow over long distances, at a speed equal to that of cells moving along the flow. Thus, the reported cell motion is not forced but only induced by external shear flow, intracellular processes such as actin polymerization or molecular motors being the real propulsive forces. Second, the speed and direction of SFICM are independently controlled, because LY294002-treated cells do not exhibit increased motility over untreated cells in the absence of the flow (data not shown). The formation of a phosphorylated phosphatidylinositol gradient by PI3K activity is therefore not a prerequisite for actin assembly at the leading edge of *D. discoideum* cells.

Discussion

This work provides evidence that a specific signaling pathway is present in *D. discoideum* that redirects the actin cytoskeleton polymerization machinery in response to external forces, resulting in cell motility. The main difference between SFICM and the usual chemotactic behavior of *D. discoideum* consists in the relative localization of the external signal and pseudopodium emission. In cAMP or folate chemotaxis, receptor stimulation induces local actin polymerization while

in SFICM, actin polymerization occurs on the side opposite to the zone of maximum stress. This is more comparable to repulsive chemotaxis, as seen (for instance) in the response of axon growth cones to diffusible chemorepellents such as netrins (Hamasaki et al., 2001; Tessier-Lavigne and Goodman, 1996).

Mechanosensitivity of *D. discoideum* cells

As for the molecular origin of the signal, three possibilities can be envisioned: (1) activation of stress-sensitive membrane channels, allowing external ions to flow in or out of the cell; (2) mechanical deformation of the actin cortex, resulting in protein recruitment at the most stressed side of the cell; or (3) the presence of a self-organizing adhesion mechanism, perturbed by mechanical peeling of the cell-substrate contact area. Stress-activated ion channels have been found in many cells, from bacteria to humans (Hamill and Martinac, 2001), which argues strongly for their presence in *D. discoideum* as well, although none has yet been reported. The second possibility recently received strong support from experiments conducted on fibroblast cytoskeleton ghosts (Sawada and Sheetz, 2002) in which application of mechanical stress results in an increased binding of paxillin, focal adhesion kinase and p130^{Cas} to focal contact structures. In *D. discoideum*, the cell edge is actually bent by shear stresses of the same order of magnitude than those inducing cell movement (Simson et al., 1998). The last possibility might be related to the biochemical mechanism controlling PtdIns(3,4,5)P_3 gradient formation itself. In mammalian cells, the activation of type I PI3Ks involves the formation of a positive feedback loop with the small Rac GTPases (Rickert et al., 2000; Weiner, 2002). Several small GTPases (Rho, Rac and Cdc42) control the organization of the actin cytoskeleton. Rac proteins are therefore at the crossroads between cell mechanics and cell chemistry, through actin polymerization dynamics and phosphoinositide phosphorylation, respectively. This positive feedback loop might explain mechanosensitivity, because many self-organizing processes are sensitive to external gradients to which they are coupled.

Because the orientation of the PtdIns(3,4,5)P_3 gradient is influenced by shear stress, the question of how the direction of the movement is controlled reduces to how external forces are coupled to the formation of this gradient. However, there must be another signal that increases cell speed modulus in response to shear stress and stabilizes the direction of cell movement. The molecular nature of this signaling pathway remains to be determined. A possible mechanism explaining how speed and

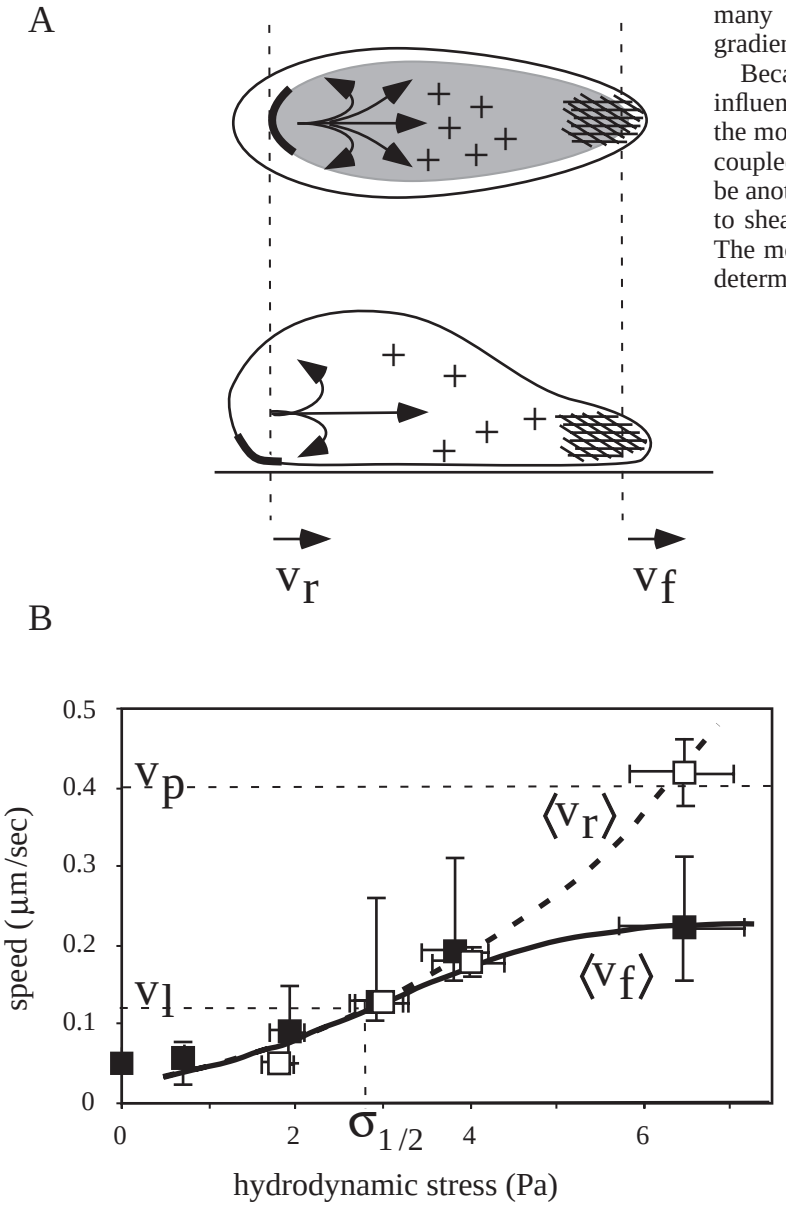

Fig. 9. Possible mechanisms of SFICM. (A) Shear stress at the cell-substrate contact area facing the flow triggers two signaling pathways. One stimulates pseudopodium emission in every direction (+), whereas the other locally inhibits pseudopodium emission near the stressed zone. This latter local signal is related to PI3K activity, because its inhibition allows pseudopodium emission against the flow. (B) Cell detachment results from the competition between SFICM and passive membrane peeling. The solid and dotted lines depict the average front and rear edge speed as a function of applied shear flow, respectively, based on the values determined in Figs 3, 5. Closed squares: cell instant speed (Fig. 3). Open squares: peeling velocity (Fig. 5). For σ=6.2 Pa, the peeling velocity is approximated by the translational velocity of rapidly detaching cells and the front velocity by the instant speed of slowly detaching cells. The threshold stress for cell detachment $\sigma_{1/2}$ corresponds to the speed at which the average front edge velocity v_f cannot adapt to the average rear edge velocity v_r; v_p designates the burst growth rate and v_l the limit in front edge velocity leading to the detachment of 50% of the cells. The dotted line corresponds to the following equation:

$$v(\sigma) = v_0(\sigma/4\sigma_0)^{1/4} \exp[(\sigma/4\sigma_0)^{1/2}] ,$$

with v_0=(1.1±0.1)×10^{-2} μm second^{-1} and σ_0=(8±0.5)×10^{-2} Pa. The rationale for using this relation to describe cell rear velocity as a function of applied or internal forces is given elsewhere (Décavé et al., 2002b). The solid line relating the front speed to the applied shear stress is hand-drawn.

direction are independently controlled is shown in Fig. 9A. The applied force would induce both the production of a diffusive second messenger and a local inhibition of pseudopodia extension. This could involve the PtdIns(3,4,5)P_3-specific phosphatase PTEN (Cantley and Neel, 1999). Upon cAMP chemotaxis, this protein indeed relocalizes to the plasma membrane in an opposite manner to PH-domain bearing proteins binding to PtdIns(3,4,5)P_3 (Funamoto et al., 2002; Iijima and Devreotes, 2002). Independent control of cell direction and speed has also been reported in other systems. Neutrophils lacking the PI3K-γ isoform exhibit alteration in motility closely similar to LY294002-treated *Dictyostelium* cells (Hannigan et al., 2002).

The behavior of cells exposed to shear flow in the presence of a PI3K inhibitor proves that the motive force is provided by the cell itself, and not by the flow. Many cells indeed move up the flow and the instant speed of these cells is comparable to that of cells moving along the flow. Pseudopodia of axenic *D. discoideum* cells have been shown to resist centrifugal forces of up to 2000 pN (Fukui et al., 2000). For comparison, the order of magnitude of forces exerted on the cells by a 1 Pa hydrodynamic shear stress is 100 pN. It is therefore not surprising that cells are able to move against such a force.

Mechanism of shear-flow-induced cell detachment

RICM visualization of cell-substrate contact areas shows that shear-flow-induced *D. discoideum* cell detachment occurs through a membrane peeling process, a hypothesis assumed but not formally proved before (Decave et al., 2002b). Furthermore, one aspect of the role of the cytoskeleton in cell adhesion is clarified. Actin cytoskeleton depolymerization indeed increases the cell detachment rate tenfold without affecting the threshold shear stress (the stress that detaches 50% of the cells). The apparent resistance of active cells to shear-stress-induced detachment is thus simply related to their ability to reattach themselves upon partial peeling of their contact area. More precisely, we observed that, for CIPC-treated cells, detachment corresponds to a transition between immobility of the cell-substrate contact area and irreversible peeling. The limit force and the relationship between the peeling velocity and the force are described by a passive model of the cell edge under tension that has been described elsewhere (Decave et al., 2002a; Garrivier et al., 2002). The speed of the front edge velocity during the fast cell-substrate area bursts (v_p=0.40 μm second^{-1}) obviously sets a limit to cell attachment under flow. In fact, the average velocity of the front edge saturates at a lower value (v_l=0.12 μm second^{-1}), corresponding to the cell velocity at the threshold shear stress for detachment ($\sigma_{1/2}$=2.6 Pa).

As far as detachment is concerned, the behavior of active cells under shear flow is therefore adequately modeled by a simple extension of the peeling model (Fig. 9B). Below the threshold, the front velocity v_f adjusts to the peeling velocity v_r and, above the threshold, the peeling velocity has to overcome a limited front velocity. This slightly modifies the expression of the detachment rate, a posteriori justifying the use of this peeling model to describe living cell detachment (Garrivier et al., 2002). Detachment of living motile cells is nevertheless intrinsically different from that of passive objects, in the sense that it is not due to the rupture of a static equilibrium but to the unbalance between two dynamic phenomena. Full understanding of cell movement, especially the alternate phases of immobility and burst at the front edge, additionally requires understanding the signaling pathways and measuring forces developed by the cell.

Physiological meaning of SFICM

The rapid increase in cell adhesion seen during burst phases is similar to the rapid spreading of suspended cells on solid substrates and to the membrane extensions enclosing the prey during phagocytic capture. Our experimental setup allows these physiological phenomena to be reproduced artificially in a controllable manner. In addition to its experimental interest, SFICM further indicates the existence of force sensitivity in *D. discoideum* cells. This mechanotaxis might play a role during developmental morphogenesis. Cells indeed move within the organism and are exposed to forces exerted by other cells (Knecht and Shelden, 1995; Shelden and Knecht, 1995). Because pseudopodia resist forces of up to 2000 pN, the forces experienced by cells in pluricellular aggregates are high enough to trigger cell responses. This rises the possibility that, in addition to the well-documented chemotactic responses, certain aspects of cell movement might be due to collective force-response behavior. In humans, professional phagocytes such as macrophages and neutrophils present a morphology and chemotactic behavior comparable to those of *D. discoideum* (Devreotes and Zigmond, 1988). These cells might also exhibit flow-induced cell motility when they are attached at the vessel walls and submitted to blood flow.

We thank P. Devreotes for providing the CRAC-GFP plasmid. We also thank G. Gerisch (Max-Planck Institüt, Martinsried, Germany) for helpful discussions. We are grateful to referees for helpful insights. This work was supported by the Commissariat à l'Energie Atomique, the Centre National de la Recherche Scientifique and the University Joseph Fourier. This work was also supported by a grant 'Adhesion Cellule-Matériaux' from the CNRS-Matériaux and the Institut National de la Santé et de la Recherche Médicale and a special grant from the Institut de la Matière Condensée (Grenoble). B. Sartor provided excellent technical assistance. E.D., S.F. and J.D. are recipients of a MENRT fellowship.

References

Asthagiri, A. R. and Lauffenburger, D. A. (2000). Bioengineering models of cell signaling. *Annu. Rev. Biomed. Eng.* **2**, 31-53.

Bereiter-Hahn, J. and Vesely, P. (1995). Reflection interference microscopy. In *Cell Biology, A Laboratory Handbook*, Vol. 3 (ed. J. Celis), pp. 54-63. Academic Press.

Buczynski, G., Grove, B., Nomura, A., Kleve, M., Bush, J., Firtel, R. A. and Cardelli, J. (1997). Inactivation of two *Dictyostelium discoideum* genes, *DdPIK1* and *DdPIK2*, encoding proteins related to mammalian phosphatidylinositide 3-kinases, results in defects in endocytosis, lysosome to postlysosome transport, and actin cytoskeleton organization. *J. Cell Biol.* **136**, 1271-1286.

Cantley, L. C. and Neel, B. G. (1999). New insights into tumor suppression: PTEN suppresses tumor formation by restraining the phosphoinositide 3-kinase/AKT pathway. *Proc. Natl. Acad. Sci. USA* **96**, 4240-4245.

Chappell, D. C., Varner, S. E., Nerem, R. M., Medford, R. M. and Alexander, R. W. (1998). Oscillatory shear stress stimulates adhesion molecule expression in cultured human endothelium. *Circ. Res.* **82**, 532-539.

Choquet, D., Felsenfeld, D. P. and Sheetz, M. P. (1997). Extracellular matrix rigidity causes strengthening of integrin-cytoskeleton linkages. *Cell* **88**, 39-48.

Chung, C. Y. and Firtel, R. A. (1999). PAKa, a putative PAK family member,

is required for cytokinesis and the regulation of the cytoskeleton in *Dictyostelium discoideum* cells during chemotaxis. *J. Cell Biol.* **147**, 559-576.

Chung, C. Y., Lee, S., Briscoe, C., Ellsworth, C. and Firtel, R. A. (2000). Role of Rac in controlling the actin cytoskeleton and chemotaxis in motile cells. *Proc. Natl. Acad. Sci. USA* **97**, 5225-5230.

Chung, C. Y., Funamoto, S. and Firtel, R. A. (2001). Signaling pathways controlling cell polarity and chemotaxis. *Trends Biochem. Sci*. **26**, 557-566.

Condeelis, J., Hall, A., Bresnick, A., Warren, V., Hock, R., Bennett, H. and Ogihara, S. (1988). Actin polymerization and pseudopod extension during amoeboid chemotaxis. *Cell Motil. Cytoskeleton* **10**, 77-90.

Cornillon, S., Pech, E., Benghezal, M., Ravanel, K., Gaynor, E., Letourneur, F., Bruckert, F. and Cosson, P. (2000). Phg1p is a nine-transmembrane protein superfamily member involved in *Dictyostelium* adhesion and phagocytosis. *J. Biol. Chem*. **275**, 34287-34292.

Decave, E., Garrivier, D., Brechet, Y., Bruckert, F. and Fourcade, B. (2002a). Peeling process in living cell movement under shear flow. *Phys. Rev. Lett.* **89**, 108101.

Decave, E., Garrivier, D., Brechet, Y., Fourcade, B. and Bruckert, F. (2002b). Shear flow-induced detachment kinetics of *Dictyostelium discoideum* cells from solid substrate. *Biophys. J*. **82**, 2383-2395.

Devreotes, P. N. and Zigmond, S. H. (1988). Chemotaxis in eukaryotic cells: a focus on leukocytes and *Dictyostelium*. *Annu. Rev. Cell. Biol*. **4**, 649-686.

Fukui, Y., Uyeda, T. Q., Kitayama, C. and Inoue, S. (2000). How well can an amoeba climb? *Proc. Natl. Acad. Sci. USA* **97**, 10020-10025.

Funamoto, S., Meili, R., Lee, S., Parry, L. and Firtel, R. A. (2002). Spatial and temporal regulation of 3-phosphoinositides by PI 3-kinase and PTEN mediates chemotaxis. *Cell* **109**, 611-623.

Garrivier, D., Decave, E., Brechet, Y., Bruckert, F. and Fourcade, B. (2002). Peeling model for cell detachment. *Eur. Phys. J. E* **8**, 79-97.

Hamasaki, T., Goto, S., Nishikawa, S. and Ushio, Y. (2001). A role of netrin-1 in the formation of the subcortical structure striatum: repulsive action on the migration of late-born striatal neurons. *J. Neurosci*. **21**, 4272-4280.

Hamill, O. P. and Martinac, B. (2001). Molecular basis of mechanotransduction in living cells. *Physiol. Rev*. **81**, 685-740.

Hannigan, M., Zhan, L., Li, Z., Ai, Y., Wu, D. and Huang, C. K. (2002). Neutrophils lacking phosphoinositide 3-kinase γ show loss of directionality during *N*-formyl-Met-Leu-Phe-induced chemotaxis. *Proc. Natl. Acad. Sci. USA* **99**, 3603-3608.

Iijima, M. and Devreotes, P. (2002). Tumor suppressor PTEN mediates sensing of chemoattractant gradients. *Cell* **109**, 599-610.

Iijima, M., Huang, Y. E. and Devreotes, P. (2002). Temporal and spatial regulation of chemotaxis. *Dev. Cell* **3**, 469-478.

Ingber, D. E. (1997). Tensegrity: the architectural basis of cellular mechanotransduction. *Annu. Rev. Physiol*. **59**, 575-599.

Jay, P. Y., Pham, P. A., Wong, S. A. and Elson, E. L. (1995). A mechanical function of myosin II in cell motility. *J. Cell Sci*. **108**, 387-393.

Kay, R. R. (2002). Chemotaxis and cell differentiation in *Dictyostelium*. *Curr. Opin. Microbiol*. **5**, 575-579.

Killirch, T., Path, P. J., Xiang, W., Bultmann, H., Rensing, L. and Vicker, M. G. (1993). The locomotion, shape and pseudopodial dynamics of unstimulated *Dictyostelium* cells are not random. *J. Cell Sci.* **106**, 1005-1013.

Knecht, D. A. and Shelden, E. (1995). Three-dimensional localization of wild-type and myosin II mutant cells during morphogenesis of *Dictyostelium*. *Dev. Biol*. **170**, 434-444.

Nerem, R. M., Alexander, R. W., Chappell, D. C., Medford, R. M., Varner, S. E. and Taylor, W. R. (1998). The study of the influence of flow on vascular endothelial biology. *Am. J. Med. Sci*. **316**, 169-175.

Newell, P. C. (1995). Signal transduction and motility of *Dictyostelium*. *Biosci. Rep*. **15**, 445-462.

Oliver, J. M., Krawiec, J. A. and Berlin, R. D. (1978). A carbamate herbicide causes microtubule and microfilament disruption and nuclear fragmentation in fibroblasts. *Exp. Cell. Res*. **116**, 229-237.

Parent, C. A., Blacklock, B. J., Froehlich, W. M., Murphy, D. B. and Devreotes, P. N. (1998). G protein signaling events are activated at the leading edge of chemotactic cells. *Cell* **95**, 81-91.

Rickert, P., Weiner, O. D., Wang, F., Bourne, H. R. and Servant, G. (2000). Leukocytes navigate by compass: roles of PI3Kγ and its lipid products. *Trends Cell Biol*. **10**, 466-473.

Riveline, D., Zamir, E., Balaban, N. Q., Schwarz, U. S., Ishizaki, T., Narumiya, S., Kam, Z., Geiger, B. and Bershadsky, A. D. (2001). Focal contacts as mechanosensors: externally applied local mechanical force induces growth of focal contacts by an mDia1-dependent and ROCK-independent mechanism. *J. Cell Biol*. **153**, 1175-1186.

Rupper, A. C., Rodriguez-Paris, J. M., Grove, B. D. and Cardelli, J. A. (2001). p110-related PI 3-kinases regulate phagosome-phagosome fusion and phagosomal pH through a PKB/Akt dependent pathway in *Dictyostelium*. *J. Cell Sci*. **114**, 1283-1295.

Sawada, Y. and Sheetz, M. P. (2002). Force transduction by *Triton* cytoskeletons. *J. Cell Biol*. **156**, 609-615.

Shelden, E. and Knecht, D. A. (1995). Mutants lacking myosin II cannot resist forces generated during multicellular morphogenesis. *J. Cell Sci.* **108**, 1105-1115.

Simson, R., Wallraff, E., Faix, J., Niewohner, J., Gerisch, G. and Sackmann, E. (1998). Membrane bending modulus and adhesion energy of wild-type and mutant cells of *Dictyostelium* lacking talin or cortexillins. *Biophys. J*. **74**, 514-522.

Tessier-Lavigne, M. and Goodman, C. S. (1996). The molecular biology of axon guidance. *Science* **274**, 1123-1133.

Theriot, J. A. and Mitchison, T. J. (1991). Actin microfilament dynamics in locomoting cells. *Nature* **352**, 126-131.

Verkhovsky, A. B., Svitkina, T. M. and Borisy, G. G. (1999). Self-polarization and directional motility of cytoplasm. *Curr. Biol*. **9**, 11-20.

Vicker, M. G. (1994). The regulation of chemotaxis and chemokinesis in *Dictyostelium* amoebae by temporal signals and spatial gradients of cyclic AMP. *J. Cell Sci.* **107**, 659-667.

Vlahos, C. J., Matter, W. F., Hui, K. Y. and Brown, R. F. (1994). A specific inhibitor of phosphatidylinositol 3-kinase, 2-(4-morpholinyl)-8-phenyl-4H-1-benzopyran-4-one (LY294002). *J. Biol. Chem*. **269**, 5241-5248.

Watts, D. J. and Ashworth, J. M. (1970). Growth of myxameobae of the cellular slime mould *Dictyostelium discoideum* in axenic culture. *Biochem. J*. **119**, 171-174.

Weber, I., Wallraff, E., Albrecht, R. and Gerisch, G. (1995). Motility and substratum adhesion of *Dictyostelium* wild-type and cytoskeletal mutant cells: a study by RICM/bright-field double-view image analysis. *J. Cell Sci*. **108**, 1519-1530.

Weijer, C. J. (1999). Morphogenetic cell movement in *Dictyostelium*. *Semin. Cell. Dev. Biol*. **10**, 609-619.

Weiner, O. D. (2002). Regulation of cell polarity during eukaryotic chemotaxis: the chemotactic compass. *Curr. Opin. Cell Biol.* **14**, 196-202.

Zamir, E. and Geiger, B. (2001). Molecular complexity and dynamics of cell-matrix adhesions. *J. Cell Sci.* **114**, 3583-3590.

Zhou, K., Takegawa, K., Emr, S. D. and Firtel, R. A. (1995). A phosphatidylinositol (PI) kinase gene family in *Dictyostelium discoideum*: biological roles of putative mammalian p110 and yeast Vps34p PI 3-kinase homologs during growth and development. *Mol. Cell. Biol*. **15**, 5645-5656.